

## Article

# A Low-Temperature Heat Output Photoactive Material-Based High-Performance Thermal Energy Storage Closed System

Xiangyu Yang<sup>1,2</sup>, Shijie Li<sup>2</sup>, Jin Zhang<sup>2</sup>, Xiaomin Wang<sup>1</sup>, Yongzhen Wang<sup>1,\*</sup> and Jianguo Zhao<sup>1,2,\*</sup>

<sup>1</sup> College of Materials Science and Engineering, Taiyuan University of Technology, Yingze West Street, Taiyuan 030024, China; yangxiangyu0039@link.tyut.edu.cn (X.Y.); wangxm62@126.com (X.W.)

<sup>2</sup> Institute of Carbon Materials Science, Shanxi Datong University, Xingyun Street, Datong 037009, China; li841974@sina.com (S.L.); zhangjin50@hrbeu.edu.cn (J.Z.)

\* Correspondence: wangyz62@163.com (Y.W.); zhaojianguo@sxdtdx.edu.cn (J.Z.)

**Abstract:** Designing and synthesizing photothermal conversion materials with better storage capacity, long-term stability as well as low temperature energy output capability is still a huge challenge in the area of photothermal storage. In this work, we report a brand new photothermal conversion material obtained by attaching trifluoromethylated azobenzene (Azof<sub>F</sub>) to reduced graphene oxide (rGO). Azof<sub>F</sub>-rGO exhibits outstanding heat storage density and power density up to 386.1 kJ·kg<sup>-1</sup> and 890.6 W·kg<sup>-1</sup>, respectively, with a long half-life (87.7 h) because of the H-bonds based on high attachment density. Azof<sub>F</sub>-rGO also exhibits excellent cycling stability and is equipped with low-temperature energy output capability, which achieves the reversible cycle of photothermal conversion within a closed system. This novel Azof<sub>F</sub>-rGO complex, which on the one hand exhibits remarkable energy storage performance as well as excellent storage life span, and on the other hand is equipped with the ability to release heat at low temperatures, shows broad prospects in the practical application of actual photothermal storage.

**Keywords:** photothermal conversion material; outstanding heat storage density; long-term storage; low temperature energy output; closed system



**Citation:** Yang, X.; Li, S.; Zhang, J.; Wang, X.; Wang, Y.; Zhao, J. A Low-Temperature Heat Output Photoactive Material-Based High-Performance Thermal Energy Storage Closed System. *Materials* **2021**, *14*, 1434. <https://doi.org/10.3390/ma14061434>

Academic Editor: Mariano Palomba

Received: 27 December 2020

Accepted: 25 February 2021

Published: 16 March 2021

**Publisher's Note:** MDPI stays neutral with regard to jurisdictional claims in published maps and institutional affiliations.



**Copyright:** © 2021 by the authors. Licensee MDPI, Basel, Switzerland. This article is an open access article distributed under the terms and conditions of the Creative Commons Attribution (CC BY) license (<https://creativecommons.org/licenses/by/4.0/>).

## 1. Introduction

With the fast development of society, people's demand for energy is increasing and the energy issue has now become one of the major problems that human beings need to deal with [1]. Solar energy has the advantages of sufficient reserves, no pollution and economical availability. Efficiently converting and storing solar energy has become an important way to overcome the current energy shortage crisis [2–5]. Recently, photothermal conversion materials have attracted extensive attention as a new method for storing solar energy [6]. Photothermal conversion materials can store solar energy in chemical bonds through photo-isomerization of units and then releasing the stored energy as thermal energy when exposed to different external stimulus, achieving photothermal conversion within a closed system. Such materials are able to effectively convert light energy into its own chemical bonds and release its stored energy while avoiding the emission of additional greenhouse gases, with the potential to achieve low-cost and large-scale industrial solar storage [7]. However, photothermal conversion materials still have the shortcomings of short storage time, low energy density and inability to achieve energy release under low temperatures, which are key factors limiting its practical application in solar thermal energy storage [8,9].

Owing to its special photoisomerization ability, good structural stability and controllable configuration recoverability, azobenzene and its derivatives with numerous applications [10,11] has received extensive research interest as a kind of photothermal conversion material [12,13]. However, due to the disadvantages of poor storage performance and storage half-life ( $\tau_{1/2}$ ) arising from low isomerization enthalpy ( $\Delta H$ ), azobenzene did not

exert its full potential in terms of photothermal conversion and storage [14]. To override the above hurdles, great efforts have been made on the basis of molecular design by introducing different substituents and increasing the interaction between molecules [15–17]. Grossman et al. [18] reported azobenzene derivatives with bulky aromatic groups as photoactive chemical heat storage materials. Owing to the introduction of bulky phenyl groups, the solid-state azobenzene derivatives not only improve the energy density but also improve the corresponding thermal stability. Bléger et al. [19] reported *o*-Fluoroazobenzenes and derivatives which exhibit an unprecedented long half-life owing to the ortho-fluorine substituent which reduces electron density around the  $-N=N-$  double bond. Despite great efforts having been made, it is still an intractable problem to apply azobenzene photothermal conversion material to practical energy storage.

Different from freely dispersed azobenzene, many azobenzene carbon materials were formed by introducing azobenzene into high-strength carbon nanomaterials forms many azobenzene carbon nanocomposites [7,20,21] accompanied by a more closely ordered structure, which have excellent storage capacity and life cycle. The templated, structure modified azobenzene enhance the intermolecular interactions while obtaining a more stable and tightly ordered structure, which jointly improved the storage capacity of azobenzene carbon materials [22,23]. In addition, because of the unique 2D structure and broad surface of graphene with numerous applications [24,25] which contributes to high attachment density, the templated azobenzene/graphene nanomaterials show broad prospects in photothermal storage [26]. Unfortunately, azobenzene carbon nanomaterials still have problems such as difficulty in releasing storage heat at low temperatures and the inability to balance energy density and half-life, which limits their further practical application [27,28]. Therefore, how to simultaneously achieve the improvement of storage capacity and life cycle with low-temperature energy output capability is still a key issue in current research.

In this work, we report a novel photothermal conversion material by attaching trifluoromethylated azobenzene ( $AzO_F$ ) to reduced graphene oxide (rGO). The storage capacity and storage life span as well as the cycling stability performance of  $AzO_F$ -rGO has made great progress.  $AzO_F$ -rGO exhibits great development potential in recyclable and long term photothermal storage.

## 2. Materials and Methods

### 2.1. Materials

3-amino-5-(trifluoromethyl)benzoic acid (99%), 3,5-dimethoxyaniline (99%), sodium nitrite (97%),  $Na_2CO_3$  (97%) and  $NaBH_4$  (97%) were purchased from Aladdin Reagent (Shanghai, China).

### 2.2. Detailed Synthesis Steps

- 3-amino-5-(trifluoromethyl)benzoic acid (1.025 g) was dissolved in the HCl solution (50 mL,  $0.5 \text{ mol}\cdot\text{L}^{-1}$ ), then  $NaNO_2$  (0.380 g) was added and reacted at ice bath for 80 min. After dissolving 3,5-dimethoxyaniline (0.765 g) in water, we slowly added the above mixture to it, adjusted the pH to 7 and reacted it in an ice bath for 4 h.  $AzO_F$  was obtained after further purification (1.255 g, 68%).
- GO was synthesized according to the literature reports [29]. First, we used NaOH ( $1 \text{ mol}\cdot\text{L}^{-1}$ ) solution to change the pH of the GO aqueous solution (300 mL,  $0.5 \text{ mg}\cdot\text{mL}^{-1}$ ) to 10, then we reacted it at  $90 \text{ }^\circ\text{C}$  for 4 h with  $NaBH_4$  (180 mg) under  $N_2$  atmosphere. When the reaction was complete, rGO was obtained by washing the mixture with water multiple times.
- $AzO_F$  (0.738 g) was dissolved in the HCl solution (60 mL,  $0.5 \text{ mol}\cdot\text{L}^{-1}$ ), then  $NaNO_2$  (0.141 g) was slowly added and reacted in an ice bath for 80 min, and the above mixture was slowly added to the rGO solution (62 mL,  $1 \text{ mg}\cdot\text{mL}^{-1}$ ). The mixture was first reacted at  $0 \text{ }^\circ\text{C}$  for 4 h and then at  $30 \text{ }^\circ\text{C}$  for 16 h.  $AzO_F$ -rGO was obtained by purifying the mixture with water and DMF multiple times.

### 2.3. Characterizations

The FT-IR was gathered from Vertex 70 (Bruker, Karlsruhe, Germany). The XRD was gathered from X'Pert Pro MPD (PANalytical, Almelo, Holland). Raman spectrum was gathered from LabRAM Aramis (HORIBA, Paris, France). The XPS was gathered from ESCALAB 250Xi (ThermoFisher, Waltham, MA, USA) using C1 s = 284.8 eV for energy calibration procedures, Operation Mode:CAE:Pass Energy 100.0 Ev, software:Thermo Advantage 5.976 and hemispherical energy analyzer were used for the test, the test vacuum was  $5 \times 10^{-9}$  Torr, the sample was fixed on the sample stage with conductive glue, the background was buckled through the smart method, and the energy calibration was performed with gold, silver and copper. The TGA was performed on STA449F5 (NETZSCH, Bavaria, Germany). TEM was gathered from Tecnai F20 (FEI, Hillsboro, Oregon, USA). SEM were gathered from SU8010 (Hitachi, Tokyo, Japan). The UV-Vis absorption spectra was performed on SPECORD 50 PLUS (ANALYTIK JENA, Jena, Germany) in the range of 250~550 nm with the resolution of 0.1 nm. The *trans*  $\rightarrow$  *cis* transition was introduced by a multiband LED lamp at 365 nm. The *cis*  $\rightarrow$  *trans* transition was introduced by a multiband LED lamp at 540 nm. The light intensity was gathered from an optical power meter (PL-MW2000, Bofeilai Technology, Beijing, China). The heat storage density was determined through differential scanning calorimetry (DSC, 214 Polyma, NETZSCH, Bavaria, Germany) under N<sub>2</sub>.

## 3. Results and Discussion

### 3.1. Chemical Structure

As shown in Figure 1a, the low-resolution TEM image of rGO exhibited a smooth structure and its electron diffraction exhibited a hexagonal lattice according to Fast Fourier Transform (FFT) patterns within Figure 1b, demonstrating its good crystallinity. Figure 1c shows that the surface of the material became rough, and the electron diffraction spot of AzO<sub>F</sub>-rGO (Figure 1d) has become a closed loop attributed to the adhesion of AzO<sub>F</sub> on rGO [30,31]. Furthermore, the SEM of AzO<sub>F</sub>-rGO (Figure 1f) shows a stacking phenomenon compared with rGO (Figure 1e). This phenomenon not only reduced the distance between adjacent graphene layers but also enhanced the intermolecular interaction, resulting in a growth in the storage capacity as well as  $\tau_{1/2}$  of AzO<sub>F</sub>-rGO [21]. In addition, it can also be concluded that the distance between layers was reduced based on the XRD results (Figure S2). After the reduction of GO, the (0 0 1) diffraction peak at 11.3° disappeared [32] and was replaced by the (0 0 2) diffraction peak at 22.9° of rGO, and the corresponding grain size was 25.51 nm based on Scherrer formula [33]. After attaching AzO<sub>F</sub> onto rGO, the 2 $\theta$  of AzO<sub>F</sub>-rGO has become to 25.2° with the grain size of 22.63 nm, which is consistent with the SEM observation (Figure 1f) [34].

The AzO<sub>F</sub>-rGO had new peaks of -N=N- (1430 cm<sup>-1</sup>) and -CF<sub>3</sub> (1140 cm<sup>-1</sup>) compared to rGO [35] according to Figure 2a. Moreover, the FT-IR spectra of AzO<sub>F</sub>-rGO and AzO<sub>F</sub> also showed peaks derived from -OH (3298 cm<sup>-1</sup>) and -C=O (1640 cm<sup>-1</sup>). It can also be seen from Figure 2a that the wavenumbers of -OH and -C=O of AzO<sub>F</sub>-rGO show a significant red shift compared to that of AzO<sub>F</sub> (3204 cm<sup>-1</sup> and 1700 cm<sup>-1</sup>), confirming the formation H-bond of AzO<sub>F</sub> on rGO [36]. XPS results also proven the successful grafting of AzO<sub>F</sub> on rGO. In addition, the characteristic peaks of AzO<sub>F</sub> at 287.5 eV and 292.5 eV corresponding to C-N and C-F bond also appeared in AzO<sub>F</sub>-rGO (Figure S3) [35]. Additionally, the fact that there were characteristic peaks of -N=N- (400.3 eV) and -CF<sub>3</sub> (688.3 eV) in AzO<sub>F</sub>-rGO also confirmed the successful bonding between AzO<sub>F</sub> and rGO [35].

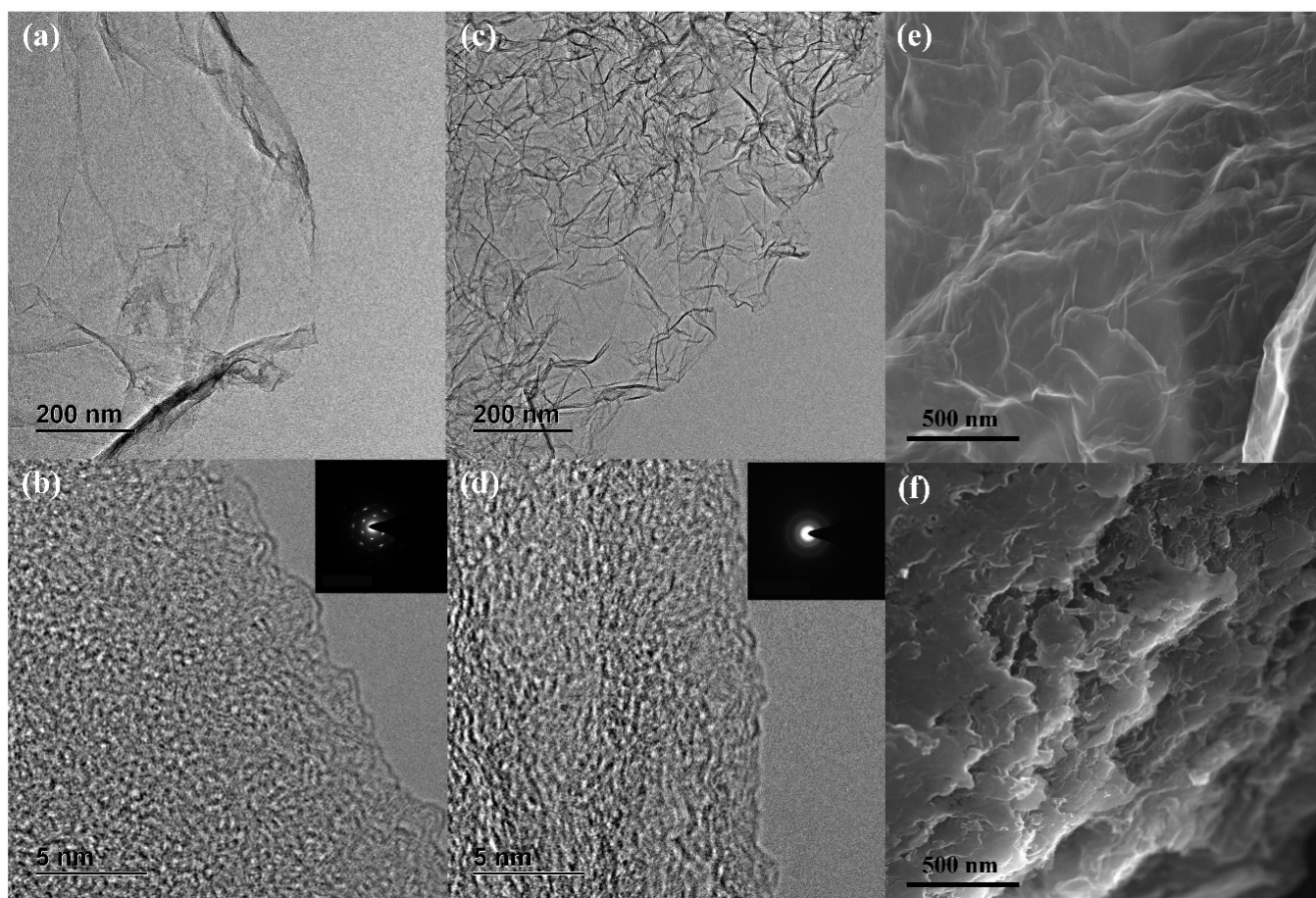


**Figure 1.** (a,c) Low resolution TEM images of rGO and AzO<sub>F</sub>-rGO, (b,d) high resolution TEM images of rGO and AzO<sub>F</sub>-rGO with FFTs, and SEM images of (e) rGO and (f) AzO<sub>F</sub>-rGO.

The high-density adhesion of AzO<sub>F</sub> onto rGO nanosheets is inextricably linked to the improvement of the performance of AzO<sub>F</sub>-rGO. The decomposition of rGO during the whole heating process was linear according to Figure 2d, and its weight loss mainly attributed to the disappearance of oxygen-containing groups [37]. The AzO<sub>F</sub> was stable before 185 °C, and its weight loss was attributed to self-decomposition. Additionally, the weight loss of AzO<sub>F</sub>-rGO was caused by the weight loss of AzO<sub>F</sub> and rGO [27]. Therefore, the attachment density ( $A_d$ ) of AzO<sub>F</sub> on rGO after different time reactions can be obtained based on Equation (1) [38].

$$D_g = \frac{R_p - R}{R_p - R_a} \times 100\% \quad (1)$$

where  $R_a$  is the residual weight percentage of AzO<sub>F</sub>,  $R$  is the residual weight percentage of AzO<sub>F</sub>-rGO,  $R_p$  is the residual weight percentage of rGO.

Table 1 shows that the attachment density ( $A_d$ ) was 1/40 after the first reaction and increased to 1/16 after the third reaction. The attachment density can also be obtained based on XPS [39]. It can also be seen from Table 1 that the results obtained by XPS and TGA were almost identical. From the above results, it can be concluded that almost every 16 carbon atoms of rGO correspond to one AzO<sub>F</sub> after the third reaction, which is better than previous research [21,40]. High adhesion density on the one hand helps to form intermolecular hydrogen bonds, while on the other hand it also enhances intermolecular interactions, which improves the storage performance of AzO<sub>F</sub>-rGO [41]. In addition, Raman spectroscopy also proved this result. It can also be seen from Figure S4 that the  $I_D/I_G$  value of AzO<sub>F</sub>-rGO-1 (1.14) and AzO<sub>F</sub>-rGO-3 (1.18) was much larger than rGO (1.08),

which indicates that the crystal structure of rGO has changed after attachment [31], proving the remarkable attachment density of AzO<sub>F</sub> on rGO.

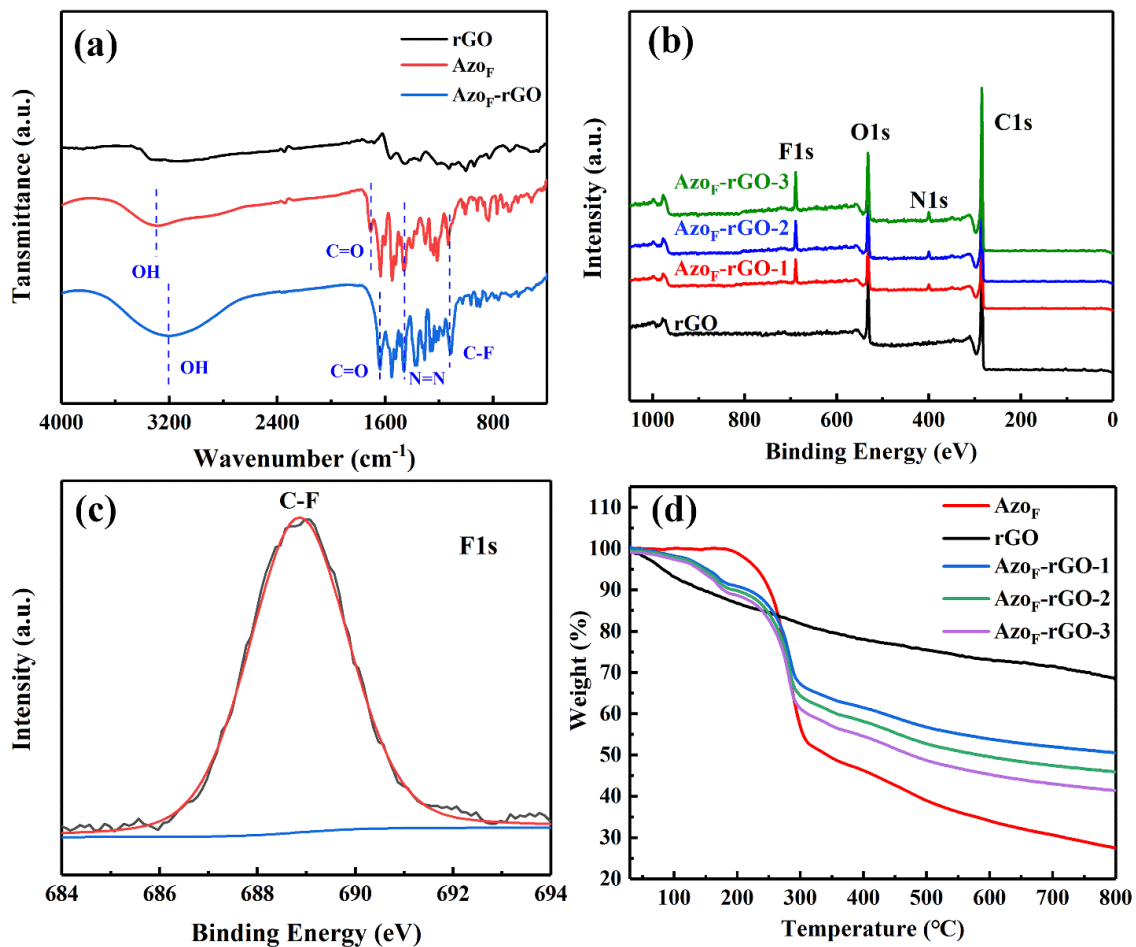


**Figure 2.** (a) FT-IR spectra of rGO, AzO<sub>F</sub> and AzO<sub>F</sub>-rGO. (b) XPS spectra of rGO and AzO<sub>F</sub>-rGO. (c) F1s XPS spectra of AzO<sub>F</sub>-rGO. (d) TGA spectra of rGO, AzO<sub>F</sub> and AzO<sub>F</sub>-rGO.

**Table 1.** A<sub>d</sub> of AzO<sub>F</sub> on rGO.

Reaction Times	TGA		XPS			A <sub>d</sub>
	D <sub>g</sub> (%) <sup>a</sup>	A <sub>d</sub>	Element Content (%)			
			C	F	O	
AzO <sub>F</sub> -rGO-1	43.41	1:40.1	77.42	4.13	15.71	1:40.2
AzO <sub>F</sub> -rGO-2	52.95	1:27.3	74.13	5.09	17.39	1:27.7
AzO <sub>F</sub> -rGO-3	65.73	1:16.0	71.07	6.64	17.90	1:16.1

<sup>a</sup> D<sub>g</sub> is the average weight percentage of AzO<sub>F</sub> in AzO<sub>F</sub>-rGO at 600 °C, 700 °C and 800 °C.

### 3.2. Cycling Stability and Storage Performance

The optical properties performance of AzO<sub>F</sub> and AzO<sub>F</sub>-rGO was investigated through time-evolved absorption spectra. It can be seen from Figure 3 that AzO<sub>F</sub>-rGO went through a *trans* → *cis* isomerization process under 365 nm ultraviolet light irradiation. Compared with AzO<sub>F</sub> (τ<sub>1/2</sub>: 195.2 min), AzO<sub>F</sub>-rGO (τ<sub>1/2</sub>: 87.7 h) takes more time to complete the isomerization process from *cis*-isomer to *trans*-isomer, indicating that AzO<sub>F</sub>-rGO has better thermal stability than pristine AzO<sub>F</sub>. The same conclusion can be drawn from the fact that the

first-order reversion rate constant ( $K_{rev}$ ) of AzO<sub>F</sub>-rGO ( $3.29 \times 10^{-6} \cdot s^{-1}$ ) was much smaller than that of AzO<sub>F</sub> ( $1.20 \times 10^{-4} \cdot s^{-1}$ ) under dark conditions derived from Equation (2) [21].

$$\ln\left(\frac{A_t - A_\infty}{A_0 - A_\infty}\right) = -k_{rev}t \quad (2)$$

where  $A_0$  is the absorption intensity of AzO<sub>F</sub>-rGO and AzO<sub>F</sub> at metastable state (*cis*-rich) irradiated by UV light,  $A_t$  is the absorbance of AzO<sub>F</sub>-rGO and AzO<sub>F</sub> reversing for “ $t$ ” time and  $A_\infty$  is the absorption intensity of AzO<sub>F</sub>-rGO and AzO<sub>F</sub> after complete *cis*-to-*trans* reversion. Moreover, compared to pristine AzO<sub>F</sub> (Figure S5), AzO<sub>F</sub>-rGO exhibited a lower isomerization degree owing to the intermolecular H-bonds and steric hindrance owing to high attachment density, resulting in a better storage performance of this material. Furthermore, the  $\Delta E_a$  value of the *cis*-isomer of AzO<sub>F</sub>-rGO (1.05 eV) was higher than that of AzO<sub>F</sub> (0.94 eV) according to Equation (3) [42], which again proves the formation of intermolecular hydrogen bonds [43].

$$E_a = -RT \ln \frac{h \ln 2}{\tau_{1/2} k_B T} \quad (3)$$

where  $E_a$  is the activation barrier for *cis*-to-*trans* isomerization process,  $T$  represents the temperature and  $\tau_{1/2}$  represents the half-life.  $k_B$ ,  $R$  and  $h$  are the Boltzman, universal gas and Plank constants. Additionally, the optical band gap of AzO<sub>F</sub>-rGO complex was estimated to be  $\sim 1.8$  eV based on the Tauc formula (Figure S6) [44]. The increase in the stability of the *cis*-isomer means extension of the life cycle of AzO<sub>F</sub>-rGO, which is directly related to the large-scale promotion of photoactive chemical heat storage materials.

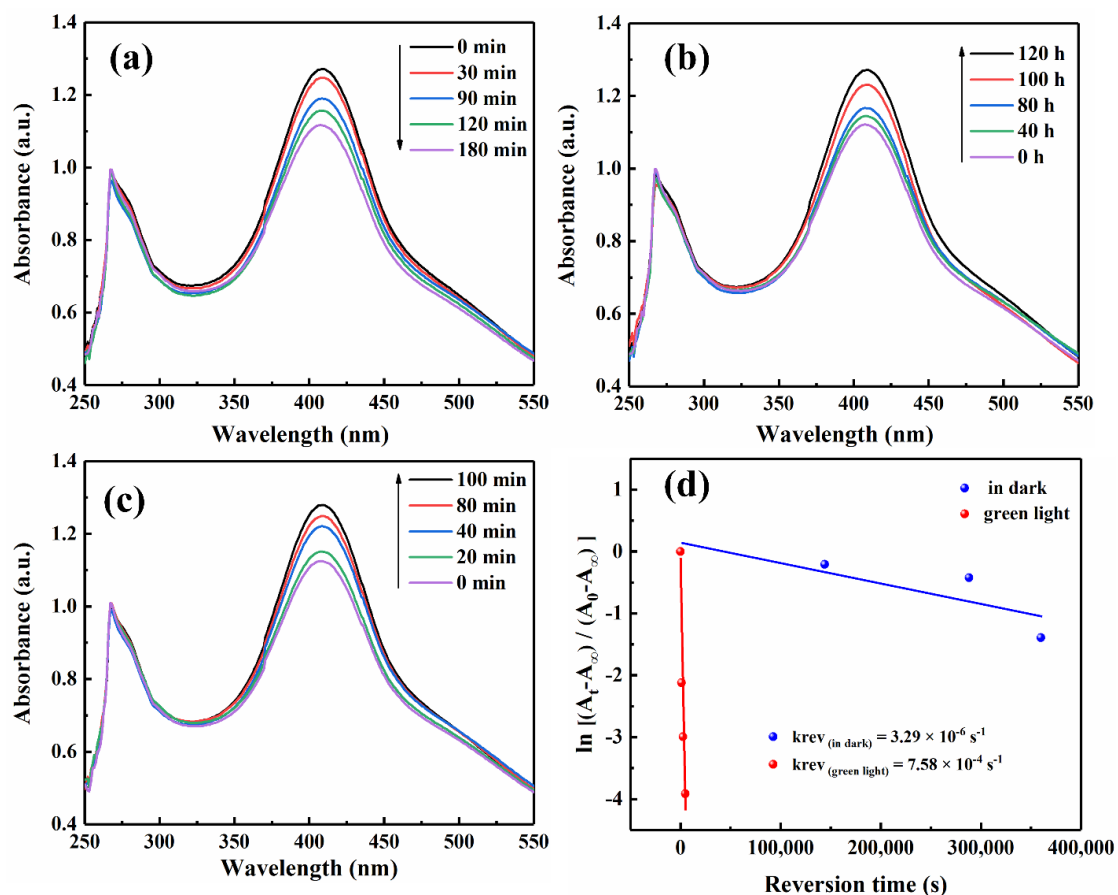


**Figure 3.** UV-Vis absorption spectra of AzO<sub>F</sub>-rGO-3 (a) under UV irradiation, (b) in dark conditions, (c) under visible light irradiation, (d) reversion rates curves of AzO<sub>F</sub>-rGO in different environments.

Similar to the length of the life cycle, whether the controllable heat release under external stimuli can be achieved is critical to the future application value of AzO<sub>F</sub>-rGO. Figure 3c showed that compared with dark conditions, the irradiation of green light (540 nm) significantly accelerated the recovery process of AzO<sub>F</sub>-rGO from *cis*-isomer to *trans*-isomer. Compared with dark conditions, the result that  $K_{rev}$  ( $7.58 \times 10^{-4} \cdot s^{-1}$ ) was significantly larger under green light irradiation also confirmed the conclusion of faster reversion. The same effect can also be achieved by absorbing heat from the external environment according to DSC. The reason for this phenomenon is that the *cis*-isomer can absorb energy from external stimuli to overcome the energy barrier of configuration reversion isomerization, thereby achieving the purpose of accelerating energy output [45,46]. The above results show that AzO<sub>F</sub>-rGO has successfully possessed the controllable heat output capability.

The stability of repeated *cis* ↔ *trans* configuration transformations of AzO<sub>F</sub>-rGO and AzO<sub>F</sub> has also been studied. It can be seen from Figure 4 that both AzO<sub>F</sub>-rGO and AzO<sub>F</sub> have no significant decrease in the absorption intensity at 407 nm after repeated irradiation of ultraviolet light (365 nm) and visible light (540 nm) for 50 times, which shows that they have outstanding isomerization stability. The AzO<sub>F</sub>-rGO can not only be stored for a long time under the premise of ensuring the storage effect, but also can control the output of the stored energy, which is essential for actual photothermal conversion.

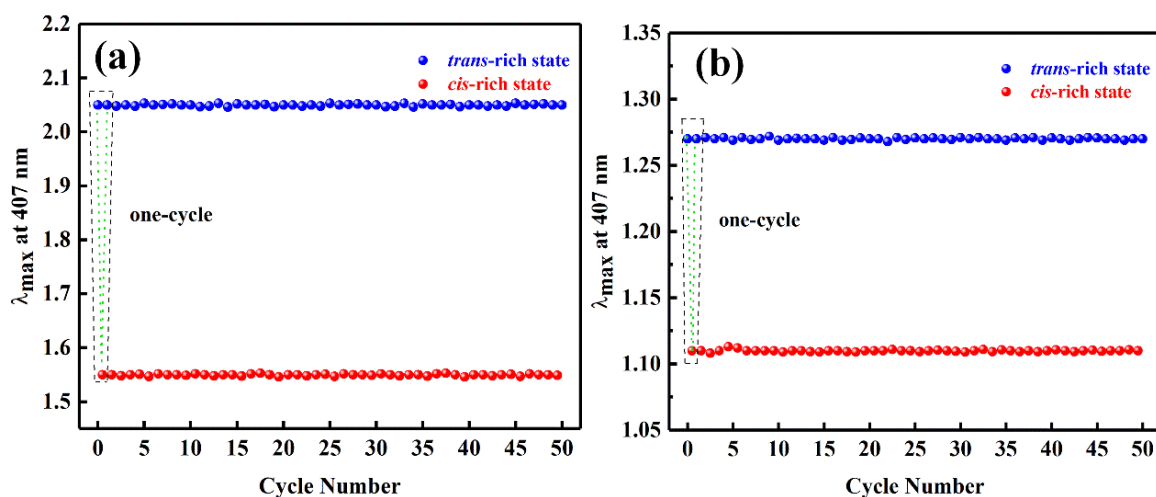


Figure 4. Stability performance of (a) AzO<sub>F</sub> and (b) AzO<sub>F</sub>-rGO-3 for 50 times.

The photothermal storage capacity of AzO<sub>F</sub> and AzO<sub>F</sub>-rGO was investigated through DSC [7]. All objects were stable between 10–140 °C based on TGA. AzO<sub>F</sub> and AzO<sub>F</sub>-rGO released significant heat under the first round of heating stimulation, but no heat was released during the second round according to Figure 5. The above results prove that the research subjects have released all the energy stored through the configuration transformation in the form of heat. Furthermore, most photothermal storage materials start to release the stored energy after 100 °C, while this kind of heat storage material can start energy output at 35 °C, which is a milestone in achieving fast energy output at lower temperatures [7].

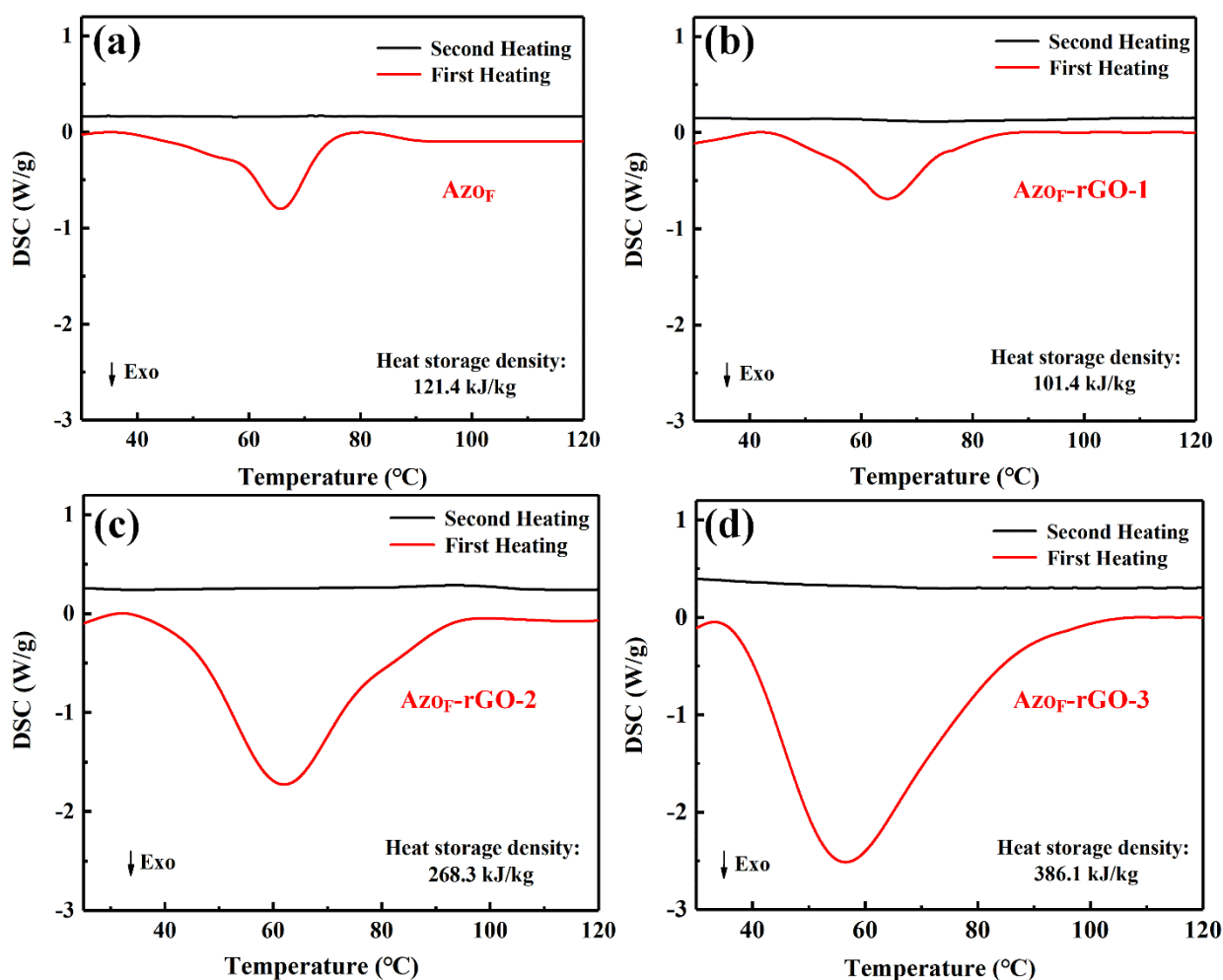


Figure 5. DSC (differential scanning calorimetry) traces of (a) Azof and (b–d) Azof-rGO after 1, 2 and 3-times reaction.

It can be seen from Figure 5 that the heat storage density of Azof-rGO-3 has reached to  $386.1 \text{ kJ kg}^{-1}$ , which shows a significant increase over Azof ( $121.4 \text{ kJ kg}^{-1}$ ). This is because of the close-packed orderly distribute of Azof on rGO as a result of high attachment density, which strengthens the intermolecular interaction [23]. In addition, high attachment density also enhances the steric hindrance and promotes the formation of H-bonds, which further increases the photothermal storage capacity [47]. The reason for Azof-rGO-1 showing less effectiveness compared to the Azof is the low attachment density, which leads to weak intermolecular interaction and therefore relatively low energy density. Moreover, the heat storage density of Azof-rGO-3 was also higher than Azof-rGO-1 and Azof-rGO-2, which shows that the attachment density was positively correlated with great storage performance.

Similar to heat storage density, power density is also a key element to measure the possibility of practical application of Azof-rGO. It can be seen from Figure 6 that the power density of Azof-rGO-3 was  $890.6 \text{ W kg}^{-1}$ , which shows a huge improvement compared to Azof ( $448.6 \text{ W kg}^{-1}$ ). Furthermore, the power density of Azof-rGO-3 was also higher than Azof-rGO-1 and Azof-rGO-2, which shows that the attachment density is directly related to the heat output performance. It is worth noting that high power density means fast output of energy, which further increases the feasibility of practical application of Azof-rGO. As shown in Table 2, the performance of Azof-rGO in many aspects has been greatly improved compared to other similar materials [7,15,48,49]. The above results demonstrate that Azof-rGO, which not only exhibits remarkable photothermal capacity but also equipped with

low temperature energy output capability, has shown great development potential in achieving the goal of efficient photothermal storage.

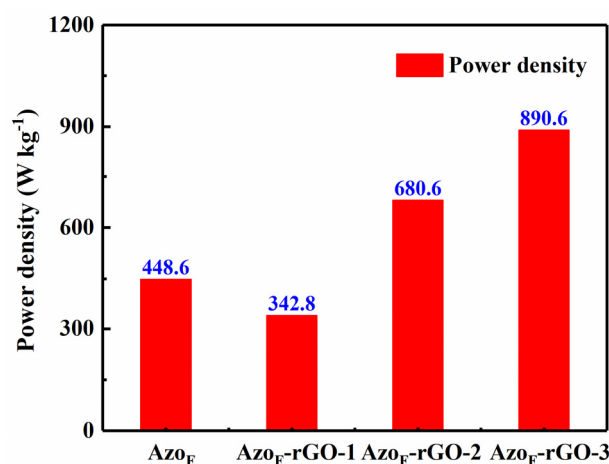


Figure 6. Power density of Azof and Azof-rGO after 1, 2 and 3-times reaction.

Table 2. Performance of different photothermal conversion materials.

Photothermal Conversion Material	Energy Density (kJ mol <sup>-1</sup> )	Power Density (W mol <sup>-1</sup> )	Half-Life (h)	Ref.
Azo-diacetylene polymer	176.2	1289.5	27.8	[48]
Azo-SWCNT complex	92.0	457.1	0.5	[7]
Azo-PCM complex	79.3	–	–	[15]
Azo-alkyl polymer	89.0	148.6	55	[49]
Azof-rGO-3 complex	367.7	848.6	87.7	This paper

#### 4. Conclusions

In summary, Azof-rGO with good photothermal storage performance, outstanding storage lifespan and low-temperature energy output capability has been proven to be a great photothermal conversion material. The formation of hydrogen bonds and the enhancement of intermolecular interactions owing to the high attachment density has simultaneously achieved the improvement of the heat storage density (max. 386.1 kJ kg<sup>-1</sup>), power density (max. 890.6 W kg<sup>-1</sup>) and half-life (up to 87.7 h) of Azof-rGO for photothermal storage. Azof-rGO also exhibits exceptional cycling stability, which realizes long-term recyclability and efficient and pollution-free utilization of solar energy in a closed system. Furthermore, Azof-rGO can start energy output at 35 °C, which shows that the goal of low-temperature energy output has been achieved. The above results indicate that Azof-rGO, combining outstanding photothermal capacity with a long-life cycle as well as low-temperature energy output capability, is a prominent photothermal conversion material with great practical application value.

**Supplementary Materials:** The following are available online at <https://www.mdpi.com/1996-1944/14/6/1434/s1>, Figure S1: <sup>1</sup>H NMR, <sup>13</sup>C NMR and <sup>19</sup>F NMR spectra of Azof, Figure S2: XRD patterns of GO, rGO, Azof-rGO, Figure S3: C1s region in XPS spectra of (a) rGO, (b) Azof-rGO and (c) N1s region in XPS spectra, Figure S4: Raman spectra, Figure S5: Time-evolved absorption spectra of Azof and Figure S6: UV-Vis absorption spectra of Azof-rGO powder at room temperature (25 °C).

**Author Contributions:** Conceptualization, X.Y. and S.L.; methodology, X.Y.; software, X.Y.; validation, X.W. and Y.W.; formal analysis, X.Y.; investigation, X.Y.; resources, J.Z. (Jin Zhang); data curation, X.Y. and S.L.; writing—original draft preparation, X.Y.; writing—review and editing, S.L.; visualization, J.Z. (Jianguo Zhao); supervision, J.Z. (Jin Zhang); project administration, J.Z. (Jianguo

Zhao); funding acquisition, J.Z. (Jin Zhang). All authors have read and agreed to the published version of the manuscript.

**Funding:** This research was funded by National Natural Science Foundation of China (Grant No. 52071192), Shanxi “1331 project” foundation for the construction of collaborative innovation center of graphene industrial application, Key Research and Development Project of Shanxi Province (Grant No. 201803D121122), Research and development projects in key areas of Guangdong Province (Grant No. 2020B0202010004), The Program for Scientific and Technological Innovation of Higher Education Institutions in Shanxi (Grant No. 2020L0477).

**Institutional Review Board Statement:** Not applicable.

**Informed Consent Statement:** Not applicable.

**Data Availability Statement:** The data presented in this study are available in [insert article or Supplementary Material].

**Conflicts of Interest:** The authors declare no conflict of interest.

## References

1. Armaroli, N.; Balzani, V. The future of energy supply: Challenges and opportunities. *Angew. Chem. Int. Ed. Engl.* **2007**, *46*, 52–66. [[CrossRef](#)] [[PubMed](#)]
2. Zhang, X.; Peng, T.; Song, S. Recent advances in dye-sensitized semiconductor systems for photocatalytic hydrogen production. *J. Mater. Chem. A* **2016**, *4*, 2365–2402. [[CrossRef](#)]
3. Aguirre, M.E.; Zhou, R.; Eugene, A.J.; Guzman, M.I.; Grela, M.A. Cu<sub>2</sub>O/TiO<sub>2</sub> heterostructures for CO<sub>2</sub> reduction through a direct Z-scheme: Protecting Cu<sub>2</sub>O from photocorrosion. *Appl. Catal. B Environ.* **2017**, *217*, 485. [[CrossRef](#)]
4. Zhou, R.; Guzman, M.I. CO<sub>2</sub> Reduction under Periodic Illumination of ZnS. *J. Phys. Chem. C* **2015**, *118*, 11649–11656. [[CrossRef](#)]
5. Moth-Poulsen, K.; Coso, D.; Börjesson, K.; Vinokurov, N.; Meier, S.K.; Majumdar, A.; Vollhardt, K.P.C.; Segalman, R.A. Molecular solar thermal (MOST) energy storage and release system. *Energy Environ. Sci.* **2012**, *5*, 8534–8537. [[CrossRef](#)]
6. Yoshida, Z.-I. New molecular energy storage systems. *J. Photochem.* **1985**, *29*, 27–40. [[CrossRef](#)]
7. Kucharski, T.J.; Ferralis, N.; Kolpak, A.M.; Zheng, J.O.; Nocera, D.G.; Grossman, J.C. Templated assembly of photoswitches significantly increases the energy-storage capacity of solar thermal fuels. *Nature Chem.* **2014**, *6*, 441–447. [[CrossRef](#)] [[PubMed](#)]
8. Kanai, Y.; Srinivasan, V.; Meier, S.K.; Vollhardt, K.P.; Grossman, J.C. Mechanism of thermal reversal of the (fulvalene)tetracarbonyl diruthenium photoisomerization: Toward molecular solar-thermal energy storage. *Angew. Chem. Int. Ed. Engl.* **2010**, *49*, 8926–8929. [[CrossRef](#)]
9. Berthiller, F.; Dall’asta, C.; Corradini, R.; Marchelli, R.; Sulyok, M.; Krska, R.; Adam, G.; Schuhmacher, R. Occurrence of deoxynivalenol and its 3-β-D-glucoside in wheat and maize. *Food Addit. Contam. Part A Chem. Anal. Control. Expo. Risk Assess* **2009**, *26*, 507–511. [[CrossRef](#)]
10. Lee, K.M.; Smith, M.L.; Koerner, H.; Tabiryan, N.; Vaia, R.A.; Bunning, T.J.; White, T.J. Photodriven, Flexural-Torsional Oscillation of Glassy Azobenzene Liquid Crystal Polymer Networks. *Adv. Funct. Mater.* **2011**, *21*, 2913–2918. [[CrossRef](#)]
11. Liu, J.; Bu, W.; Pan, L.; Shi, J. NIR-triggered anticancer drug delivery by upconverting nanoparticles with integrated azobenzene-modified mesoporous silica. *Angew. Chem. Int. Ed. Engl.* **2013**, *52*, 4375–4379. [[CrossRef](#)] [[PubMed](#)]
12. Sun, L.; Gao, F.; Shen, D.; Liu, Z.; Yao, Y.; Lin, S. Rationally designed hyperbranched azopolymer with temperature, photo and pH responsive behavior. *Polym. Chem.* **2018**, *9*, 2977–2983. [[CrossRef](#)]
13. Wang, G.; Yuan, D.; Yuan, T.; Dong, J.; Feng, N.; Han, G. A visible light responsive azobenzene-functionalized polymer: Synthesis, self-assembly, and photoresponsive properties. *J. Polym. Sci. Part A Polym. Chem.* **2015**, *53*, 2768–2775. [[CrossRef](#)]
14. Iii, J.O.; Lawrence, J.; Yee, G.G. Photochemical storage potential of azobenzenes. *Sol. Energy* **1983**, *30*, 271–274.
15. Han, G.G.D.; Li, H.; Grossman, J.C. Optically-controlled long-term storage and release of thermal energy in phase-change materials. *Nat. Commun.* **2017**, *8*, 1446. [[CrossRef](#)]
16. Joshi, D.K.; Mitchell, M.J.; Bruce, D.; Lough, A.J.; Yan, H. Synthesis of cyclic azobenzene analogues. *Tetrahedron* **2012**, *68*, 8670–8676. [[CrossRef](#)]
17. Weston, C.E.; Richardson, R.D.; Haycock, P.R.; White, A.J.; Fuchter, M.J. Arylazopyrazoles: Azoheteroarene photoswitches offering quantitative isomerization and long thermal half-lives. *J. Am. Chem. Soc.* **2014**, *136*, 11878–11881. [[CrossRef](#)]
18. Cho, E.N.; Zhitomirsky, D.; Han, G.G.; Liu, Y.; Grossman, J.C. Molecularly Engineered Azobenzene Derivatives for High Energy Density Solid-State Solar Thermal Fuels. *ACS Appl. Mater. Interfaces* **2017**, *9*, 8679–8687. [[CrossRef](#)]
19. Blegler, D.; Schwarz, J.; Brouwer, A.M.; Hecht, S. o-Fluoroazobenzenes as readily synthesized photoswitches offering nearly quantitative two-way isomerization with visible light. *J. Am. Chem. Soc.* **2012**, *134*, 20597–20600. [[CrossRef](#)]
20. Lennartson, A.; Roffey, A.; Moth-Poulsen, K. Designing photoswitches for molecular solar thermal energy storage. *Tetrahedron Lett.* **2015**, *56*, 1457–1465. [[CrossRef](#)]
21. Feng, Y.; Liu, H.; Luo, W.; Liu, E.; Zhao, N.; Yoshino, K.; Feng, W. Covalent functionalization of graphene by azobenzene with molecular hydrogen bonds for long-term solar thermal storage. *Sci. Rep.* **2013**, *3*, 3260. [[CrossRef](#)]

22. Kurihara, S.; Nomiyama, S.; Nonaka, T. Photochemical control of the macrostructure of cholesteric liquid crystals by means of photoisomerization of chiral azobenzene molecules. *Chem. Mater.* **2001**, *13*, 1992–1997. [[CrossRef](#)]
23. Kolpak, A.M.; Grossman, J.C. Hybrid chromophore/template nanostructures: A customizable platform material for solar energy storage and conversion. *J. Chem. Phys.* **2013**, *138*, 034303. [[CrossRef](#)]
24. Wu, J.; Yang, Y.; Qu, Y.; Jia, L.; Zhang, Y.; Xu, X.; Chu, S.T.; Little, B.E.; Morandotti, R.; Jia, B.; et al. 2D Layered Graphene Oxide Films Integrated with Micro-Ring Resonators for Enhanced Nonlinear Optics. *Small* **2020**, *16*, 1906563. [[CrossRef](#)]
25. Wu, J.; Yang, Y.; Qu, Y.; Xu, X.; Liang, Y.; Chu, S.T.; Little, B.E.; Morandotti, R.; Jia, B.; Moss, D.J. Graphene Oxide Waveguide and Micro-Ring Resonator Polarizers. *Laser Photonics Rev.* **2019**, *13*, 1900056. [[CrossRef](#)]
26. Wu, S.; Butt, H.-J. Solar-Thermal Energy Conversion and Storage Using Photoresponsive Azobenzene-Containing Polymers. *Macromol. Rapid Commun.* **2020**, *41*, 1900413. [[CrossRef](#)] [[PubMed](#)]
27. Zhang, X.; Feng, Y.; Huang, D.; Li, Y.; Feng, W. Investigation of optical modulated conductance effects based on a graphene oxide–azobenzene hybrid. *Carbon* **2010**, *48*, 3236–3241. [[CrossRef](#)]
28. Wang, Z.; Li, Z.-x.; Liu, Z. Photostimulated reversible attachment of gold nanoparticles on multiwalled carbon nanotubes. *J. Phys. Chem. C* **2009**, *113*, 3899–3902. [[CrossRef](#)]
29. Hummers, W.S.; Offeman, R.E. Preparation of Graphitic Oxide. *J. Am. Chem. Soc.* **1958**, *80*, 1339. [[CrossRef](#)]
30. An, X.; Simmons, T.J.; Shah, R.; Wolfe, C.S.; Lewis, K.M.; Washington, M.; Nayak, S.K.; Talapatra, S.; Kar, S. Stable Aqueous Dispersions of Noncovalently Functionalized Graphene from Graphite and their Multifunctional High-Performance Applications. *Nano Lett.* **2010**, *10*, 4295–4301. [[CrossRef](#)]
31. Englert, J.M.; Dotzer, C.; Yang, G.; Schmid, M.; Papp, C.; Gottfried, J.M.; Steinruck, H.; Spiecker, E.; Hauke, F.; Hirsch, A. Covalent bulk functionalization of graphene. *Nat. Chem.* **2011**, *3*, 279–286. [[CrossRef](#)] [[PubMed](#)]
32. Marcano, D.C.; Kosynkin, D.V.; Berlin, J.M.; Sinitskii, A.; Sun, Z.; Slesarev, A.; Alemany, L.B.; Lu, W.; Tour, J.M. Improved Synthesis of Graphene Oxide. *ACS Nano* **2010**, *4*, 4806–4814. [[CrossRef](#)] [[PubMed](#)]
33. Lim, D.J.; Marks, N.A.; Rowles, M.R. Universal Scherrer equation for graphene fragments. *Carbon* **2020**, *162*, 475–480. [[CrossRef](#)]
34. Li, D.; Muller, M.B.; Gilje, S.; Kaner, R.B.; Wallace, G.G. Processable aqueous dispersions of graphene nanosheets. *Nat. Nanotechnol.* **2008**, *3*, 101–105. [[CrossRef](#)]
35. Min, M.; Bang, G.S.; Lee, H.; Yu, B. A photoswitchable methylene-spaced fluorinated aryl azobenzene monolayer grafted on silicon. *Chem. Commun.* **2010**, *46*, 5232–5234. [[CrossRef](#)]
36. Gearba, R.I.; Lehmann, M.; Levin, J.; Ivanov, D.A.; Koch, M.H.J.; Barbera, J.; Debije, M.G.; Piris, J.; Geerts, Y. Tailoring discotic mesophases: Columnar order enforced with hydrogen bonds. *Adv. Mater.* **2003**, *15*, 1614–1618. [[CrossRef](#)]
37. Zhang, X.; Feng, Y.; Lv, P.; Shen, Y.; Feng, W. Enhanced reversible photoswitching of azobenzene-functionalized graphene oxide hybrids. *Langmuir* **2010**, *26*, 18508–18511. [[CrossRef](#)]
38. Zhang, B.; Zhang, Y.; Peng, C.; Yu, M.; Li, L.; Deng, B.; Hu, P.; Fan, C.; Li, J.; Huang, Q. Preparation of polymer decorated graphene oxide by  $\gamma$ -ray induced graft polymerization. *Nanoscale* **2012**, *4*, 1742–1748. [[CrossRef](#)]
39. Yu, D.S.; Kuila, T.; Kim, N.H.; Khanra, P.; Lee, J.H. Effects of covalent surface modifications on the electrical and electrochemical properties of graphene using sodium 4-aminoazobenzene-4'-sulfonate. *Carbon* **2013**, *54*, 310–322. [[CrossRef](#)]
40. Kim, M.; Safron, N.S.; Huang, C.; Arnold, M.S.; Gopalan, P. Light-driven reversible modulation of doping in graphene. *Nano Lett.* **2012**, *12*, 182–187. [[CrossRef](#)] [[PubMed](#)]
41. Bandara, H.M.D.; Burdette, S.C. Photoisomerization in different classes of azobenzene. *Chem. Soc. Rev.* **2012**, *41*, 1809–1825. [[CrossRef](#)]
42. Samanta, S.; Beharry, A.A.; Sadowski, O.; McCormick, T.M.; Babalhavaeji, A.; Tropepe, V.; Woolley, G.A. Photoswitching azo compounds in vivo with red light. *J. Am. Chem. Soc.* **2013**, *135*, 9777–9784. [[CrossRef](#)] [[PubMed](#)]
43. Kolpak, A.M.; Grossman, J.C. Azobenzene-Functionalized Carbon Nanotubes As High-Energy Density Solar Thermal Fuels. *Nano Lett.* **2011**, *11*, 3156–3162. [[CrossRef](#)] [[PubMed](#)]
44. Zhang, G.; Amani, M.; Chaturvedi, A.; Tan, C.; Bullock, J.; Song, X.; Kim, H.; Lien, D.H.; Scott, M.C.; Zhang, H. Optical and electrical properties of two-dimensional palladium diselenide. *Appl. Phys. Lett.* **2019**, *114*, 253102. [[CrossRef](#)]
45. Yang, Y.; Hughes, R.P.; Aprahamian, I. Visible Light Switching of a BF<sub>2</sub>-Coordinated Azo Compound. *J. Am. Chem. Soc.* **2012**, *134*, 15221–15224. [[CrossRef](#)]
46. Siewertsen, R.; Neumann, H.; Buchheimstehn, B.; Herges, R.; Nather, C.; Renth, F.; Temps, F. Highly Efficient Reversible Z–E Photoisomerization of a Bridged Azobenzene with Visible Light through Resolved S<sub>1</sub>( $n\pi^*$ ) Absorption Bands. *J. Am. Chem. Soc.* **2009**, *131*, 15594–15595. [[CrossRef](#)]
47. Liu, Y.; Grossman, J.C. Accelerating the Design of Solar Thermal Fuel Materials through High Throughput Simulations. *Nano Lett.* **2014**, *14*, 7046–7050. [[CrossRef](#)] [[PubMed](#)]
48. Han, G.D.; Park, S.S.; Liu, Y.; Zhitomirsky, D.; Cho, E.; Dincă, M.; Grossman, J.C. Photon energy storage materials with high energy densities based on diacetylene–azobenzene derivatives. *J. Mater. Chem. A* **2016**, *4*, 16157–16165. [[CrossRef](#)]
49. Zhitomirsky, D.; Cho, E.; Grossman, J.C. Solid-State Solar Thermal Fuels for Heat Release Applications. *Adv. Energy Mater.* **2016**, *6*, 1502006. [[CrossRef](#)]